Inorganic Chemistry

Article

pubs.acs.org/IC

Electronic Pseudogap-Driven Formation of New Double-Perovskite-like Borides within the $Sc_2Ir_{6-x}T_xB$ (T = Pd, Ni; x = 0−6) Series

Martin Hermus,[†] Jan P. Scheifers,[†] Rachid Touzani, and Boniface P. T. Fokwa*

Institute of Inorganic Chemistry, RWTH Aachen University, 52056 Aachen, Germany

Supporting Information

ABSTRACT: Analysis of the electronic density of states of the hypothetical ternary double-perovskite-like phases "Sc_2T_6B (T = Ir, Pd, Ni)" reveals the presence of deep and large pseudogaps between 61 and 68 valence electrons (VE) as well as a strong peak at 69 VEs. Subsequently, crystal orbital Hamilton population (COHP) bonding analysis shows that the heteroatomic T−B and Sc−T interactions are optimized in Sc_2Ir_6B (63 VE) but not in "Sc_2Pd_6B (69 VE)" and "Sc_2Ni_6B (69 VE)", thus indicating less stability for these VE-richer phases. These findings point out the possibility of discovering new double-perovskite-like borides through chemical substitution and lead to the study of the $Sc_2Ir_{6-x}Pd_xB$ and $Sc_2Ir_{6-x}Ni_xB$ (x = 0−6; VE = 63−69) series, for which powder samples and single crystals were synthesized by arc melting the elements. Superstructure reflections were observed in the powder diffractograms of $Sc_2Ir_{6-x}Pd_xB$ and $Sc_2Ir_{6-x}Ni_xB$ for x = 0−5 and VE = 63−68, thereby showing that these phases crystallize in the double-perovskite-like Ti_2Rh_6B-type structure (space group $Fm\bar{3}m$, Z = 4). Single-crystal and Rietveld refinement results confirm and extend these findings because Pd (or Ni) is found to mix exclusively with Ir in all quaternary compositions. For x = 6, no superstructure reflections were observed, in accordance with the theoretical expectation for the 69 VE phases.

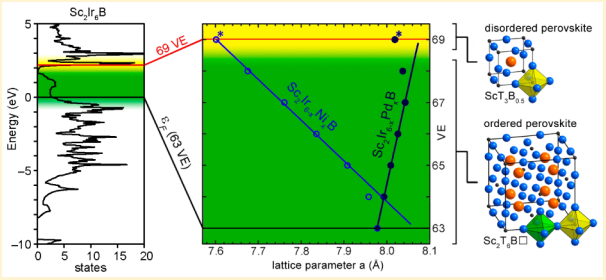

INTRODUCTION

Metal-rich phases (AM_3X, where A and M are metals and X is either N, C, or B) crystallizing with the cubic perovskite-like (also called antiperovskite) structure still remain in the focus of experimentalists and theoreticians because of their simple crystal structure and the huge variety of physical properties observed.[1] Because these phases have often been reported as non-stoichiometric, especially at the light element sites (AM_3X_y), it is very important to extend the knowledge about this structure class through careful examination of their diffraction patterns, as has been successfully done for their oxide counterpart.

The study of these metal-rich borides (AM_3B_y) has particularly been attractive in the materials sciences community because of their interesting physical properties.[2−7] Ti_2Rh_6B, described as a vacancy containing double-perovskite-like structure, is the first phase in which boron ordering was observed by X-ray diffraction methods.[8] Electron diffraction on some nonstoichiometric phases, namely, $CeRh_3B_y$ ($0.4 \le y \le 0.5$)[9] and $ScRh_3B_x$ ($0.5 \le y \le 0.75$),[10] revealed the presence of $^1/_2$ $^1/_2$ $^1/_2$ superstructure reflections and minor satellite ones, which also points to boron ordering and indicates that many nonstoichiometric perovskite-like phases are only average structures. However, single-crystal or powder X-ray diffractometry are needed to confirm these superstructures in order to find the real chemical formulas. Zr_2Ir_6B,[11] formerly known as nonstoichiometric $ZrIr_3B_{0.5}$,[5] was reformulated recently because of the observation of $^1/_2$ $^1/_2$ $^1/_2$ superstructure reflections by single-crystal and powder X-ray diffraction. The discovery of these superstructure reflections in a long-known phase allow one to assume that, of the multiple known nonstoichiometric perovskites, some may, in fact, crystallize with the 8-fold supercell as well. Additionally, the electronic structure calculations performed on Zr_2Ir_6B showed a large pseudogap in the density of states (DOS) of this phase (see Figure 5 in ref11). This discovery suggests the possibility of finding new double-perovskite borides by electronically adjusting the Fermi level within the pseudogap through chemical substitution. Recently, the presence of a pseudogap combined with a rigid band approximation was successfully used to predict new $Ti_3Co_5B_2$-type metal-rich borides: For example, the pseudogap found in the DOS of $Nb_3Ru_5B_2$[12] was exploited for the discovery of the complex "$Nb_2MRu_5B_2$" (M = Sc−Ni) series, in which the rigid band approximation worked nearly to perfection and led to three different chemical formulas along the series: $(Nb_{2-x}Sc_x)^{4g}Nb^{2a}Ru_5B_2$ ($1 \le x < 2$), $Nb_{3-x}M_xRu_5B_2$ (M = Ti, V; $x \approx 1$), and $Nb_{2+x}M_{1-x}Ru_5B_2$ (M = Cr, Mn, Fe, Co, Ni; $0 < x \le 0.5$).[13] Additionally, some other ternary and quaternary phases of $Ti_3Co_5B_2$-type structure have been shown to strictly follow the rigid band model.[14,15] The pseudogap found in the DOS of Zr_2Ir_6B, which has 65 valence electrons (VE), ranges from 61 VE up to 68 VE, so it should be possible to remove or add electrons by element substitution within this VE range without destabilizing the superstructure if electronic factors dominate over size effects.

Received: February 6, 2015
Published: April 7, 2015

DOI: 10.1021/acs.inorgchem.5b00292
Inorg. Chem. 2015, 54, 4056−4063

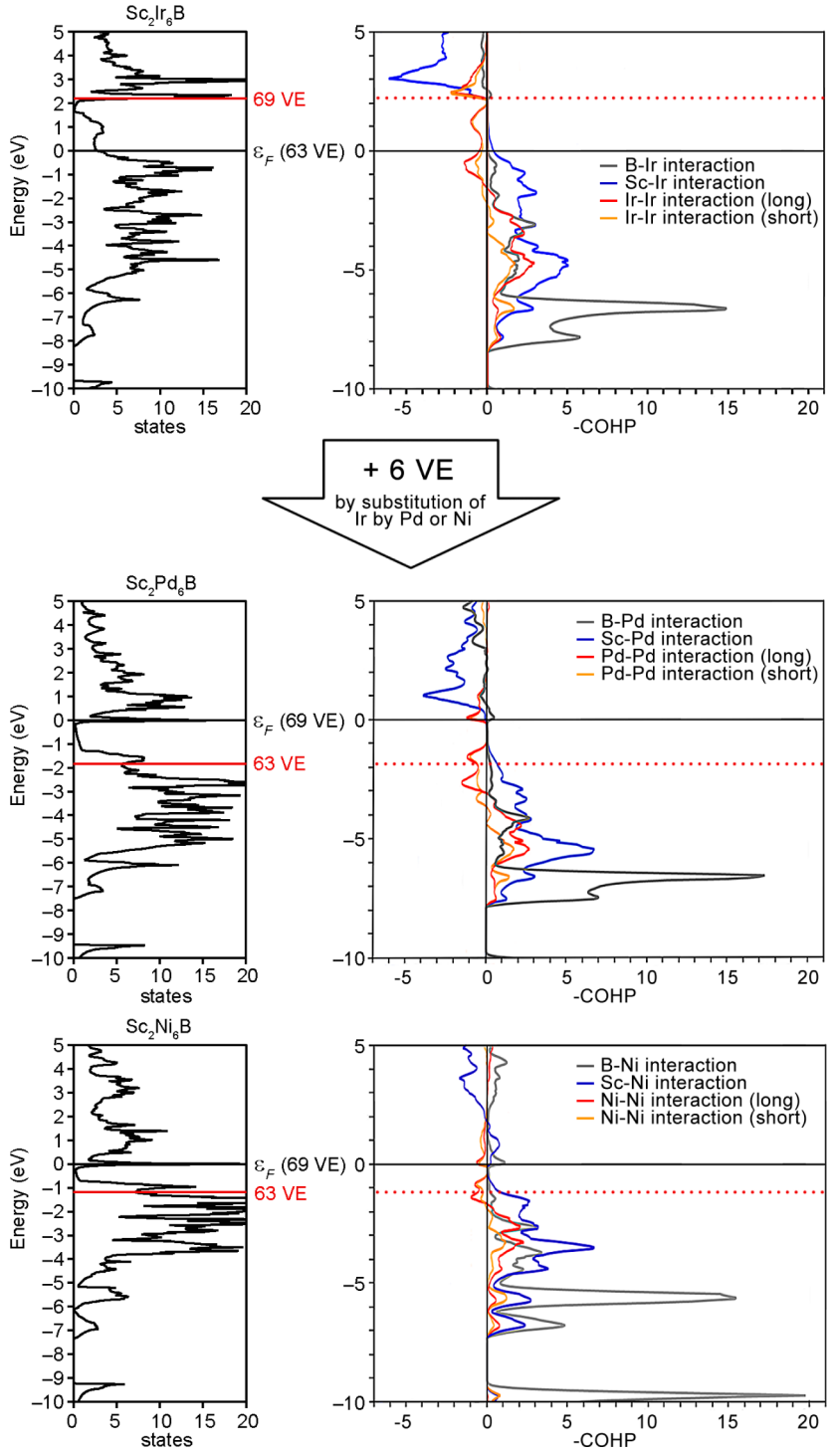

Figure 1. DOS (on the left) and COHP (on the right) plots of Sc_2Ir_6B (63 VE, top) and the hypothetical phases Sc_2Pd_6B (69 VE, middle) and Sc_2Ni_6B (69 VE, bottom). For the DOS, the predicted Fermi level of the other phase is drawn in red. The B−T interactions are given in gray, Sc−T interactions in blue, T−T interactions (long) in orange, and T−T interactions (short) in red for the COHP plots. (T = Ir, Pd, Ni).

On this account, we have resynthesized and characterized the already known nonstoichiometric phase $ScIr_3B_y$[4] for $y = 0.5$ (or Sc_2Ir_6B with 63 VE), in particular because the atomic sizes of Sc and Zr are comparable and thus electronic effects should dominate. Thereafter, we tuned the VE count by a stepwise substitution of Ir by Pd or Ni, leading not only to several quaternary compositions within the predicted VE range but also to the hypothetical ternary phases "Sc_2Pd_6B (69 VE)" and "Sc_2Ni_6B (69 VE)", whose VE counts fall outside of the predicted VE range and which have already been reported as $ScPd_3B_{0.5}$[1a] and $ScNi_3B_{0.5}$,[16] respectively. The advantage of this substitution is that, besides the electronic effect (VE tuning), the size effect will also be studied because Ir will be substituted not only by the larger Pd but also by the smaller Ni.

RESULTS AND DISCUSSION

DOS of the Hypothetical "Sc_2T_6B (T = Ir, Pd, Ni)" Compounds. The electronic structures of the hypothetical

DOI: 10.1021/acs.inorgchem.5b00292
Inorg. Chem. 2015, 54, 4056−4063

"Sc_2T_6B (T = Ir, Pd, Ni)" borides with double-perovskite-like structure (Ti_2Rh_6B type) have been calculated using the local density approximation within the tight-binding linear muffin-tin orbital method (TB-LMTO) code. Figure 1 shows the DOSs of the three compounds, and each of them has a pseudogap around the Fermi level (E_F). The effect of 5d−4d−3d substitution within the series is obvious as the three DOSs differ from each other mainly because of the different signatures arising from the 5d (Ir), 4d (Pd), and 3d (Ni) bands: While the 3d states of Ni are more contracted, the 5d states of Ir are more dispersed, whereas the 4d states of Pd lie in between. The consequences are three differently built pseudogaps: That of "Sc_2Ir_6B" (Figure 1, top left) is the largest but also has the fewest states around E_F, while that of "Sc_2Ni_6B" (Figure 1, bottom left) is the narrowest but with the most states around E_F and that of "Sc_2Pd_6B" (Figure 1, middle left) lies in between. Nevertheless, each pseudogap ranges between 61 and 68 VE. The Ni and Pd phases have 69 VEs each, and thus their Fermi levels are found outside of the pseudogap and on a DOS peak, indicating electronic instability, whereas that of the Ir phase lies just at the lower end of the pseudogap, making the phase plausible and more likely to crystallize with the double-perovskite-like structure.

The bonding situation in the ternary systems "Sc_2T_6B" with T = Ir, Ni, or Pd was analyzed in detail by applying the concept of crystal orbital Hamilton populations (COHPs). The interactions of interest are B−T, Sc−T, and T−T. Other interactions such as Sc−B are too weak to be considered as bonding. Because there are T_6 octahedra filled by boron and empty T_6 octahedra, there are two T−T distances that have to be taken into account. The shorter one occurs in the empty octahedron, while the larger one builds the filled octahedron.

A look at the COHP plots of Sc_2Ir_6B (Figure 1, top right) reveals strong B−Ir bonding interactions up to E_F with two major peaks below $E \approx -6$ eV. Between E_F and $E \approx 2$ eV, nonbonding states are observed, and above $E \approx 2$ eV, very few antibonding states are present. This is basically an optimized COHP with bonding states below and antibonding ones above E_F.

The Sc−Ir interaction has a bonding character up to $E \approx 0.5$ eV, followed by nonbonding character up to $E \approx 2$ eV. Above this energy, the interaction becomes strongly antibonding with a peak at $E \approx 3$ eV. The Sc−Ir interactions are not as strong as the B−Ir interactions, but they occur twice as often.

The situation for the Ir−Ir interactions is different. They are weaker than the other interactions, and the transition from bonding to antibonding character occurs below E_F at $E \approx -2$ eV, resulting in antibonding states at E_F. Around $E \approx 2$ eV, nonbonding states are present. The difference between long and short Ir−Ir interactions is small, with slightly stronger interaction observed for the shorter distance.

In conclusion, the optimized heteroatomic B−Ir and Sc−Ir interactions, which are strongly bonding, are mainly responsible for the structural stability of Sc_2Ir_6B. The Ir−Ir interactions are weaker and antibonding around E_F as well as in the pseudogap range. The pseudogap range visible in the DOS begins just below E_F through $E \approx 2$ eV. The B−Ir interactions in this region are basically nonbonding, while the Sc−Ir interactions are just slightly bonding and the Ir−Ir interactions therein are considerably antibonding. There is a small region at $E \approx 2$ eV, which is enclosed by antibonding Ir−Ir interactions, with purely nonbonding states at the upper limit of the pseudogap. This finding is very similar to the situation found in Zr_2Ir_6B (compare Figure 5 in ref 11). There are slight changes in the Sc−Ir interactions compared to the Zr−Ir interactions because a 3d metal replaces a 4d metal, but the overall shape of all interactions stays the same. A noteworthy observation is the fact that the position of E_F in Sc_2Ir_6B is slightly lower than that for Zr_2Ir_6B: In Zr_2Ir_6B, the Fermi level is located at a small peak inside the pseudogap, but in Sc_2Ir_6B, it is slightly lower and lies in a local minimum. The reason is the different number of VE. The isostructural substitution of Zr by Sc decreases the number of VE by two, resulting in a shifting of the Fermi level to lower energies, as predicted by the rigid band model.

Let us now apply the rigid band model to the COHP curves of Sc_2Ir_6B and shift its Fermi level upward from 63 to 69 VE: As Figure 1 (top) shows, no bonding interactions are added in the process, while substantial antibonding interactions are, thus destabilizing the VE-richer structures. The situation is even worse for the extreme cases "Sc_2Pd_6B" or "Sc_2Ni_6B" with 69 VE, because at this VE count heteroatomic antibonding interactions are additionally found; thus, according to this analysis, these phases will be more unstable than the VE-poorer ones. In the next step, the COHP curves of the hypothetical "Sc_2Pd_6B" and "Sc_2Ni_6B" phases were calculated (see Figure 1, middle and bottom) on the basis of the Ti_2Rh_6B-type structure, the results of which confirm the above prediction of the rigid band model applied to the COHPs of Sc_2Ir_6B.

$Sc_2Ir_{6-x}Pd_xB$ Series. Analysis of the powder diffractograms of the $Sc_2Ir_{6-x}Pd_xB$ series (x = 0−6) shows that in all cases a perowskite-like structure has been obtained. The x = 0 and 3 compositions are contaminated with small amounts of $Ir_{1-x}Pd_x$ ($0 \le x \le 1$, Cu-type structure, space group $Fm\bar{3}m$). The powder diffractograms of all compositions within the series are plotted in Figure 2, and the 2θ range, in which two of the superstructure

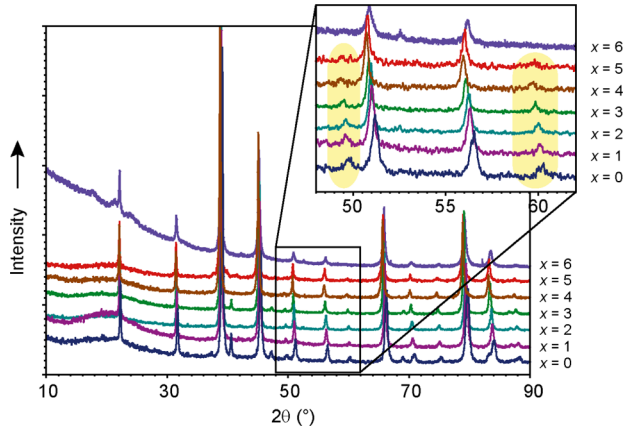

Figure 2. Powder patterns (Cu Kα_1 radiation) of the $Sc_2Ir_{6-x}Pd_xB$ series (x = 0−6). The 2θ range, in which two of the superstructure reflections [(331) and (333)] are located, is magnified.

reflections [(331) and (333)] should be located, is magnified. A closer look at these powder diffractograms reveals that the superstructure reflections exist for the compositions with x = 0, 1, 2, 3, 4 and 5 but not for x = 6. After indexation of the main reflections of the already known x = 0 phase, the resulting lattice parameter, a = 3.9827(5) Å, lies between those of $ScIr_3$ (Cu_3Au type, a = 3.90 Å),[17] and $ScIr_3B_{1-y}$ ($SrTiO_3$ type, a = 3.999 Å),[4] as expected. However, taking into account the superstructure reflections, the lattice parameters are doubled, indicating that this phase should crystallize with the double-perovskite-like Ti_2Rh_6B-type structure instead. For x = 6, no superstructure was observed, and the refined lattice parameter, a = 4.0073(4) Å, is larger than that of the binary phase $ScPd_3$ (Cu_3Au type), for which values of

DOI: 10.1021/acs.inorgchem.5b00292
Inorg. Chem. 2015, 54, 4056−4063

3.958 and 3.982 Å are present in the literature,[18] therefore indicating the successful incorporation of boron in the octahedral site, as reported already.[1a] Figure 3 shows the lattice parameters

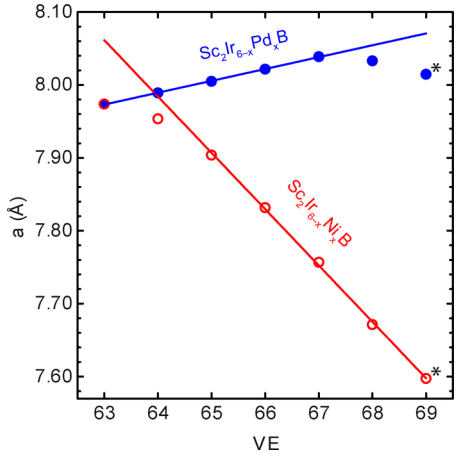

Figure 3. Lattice parameter a as a function of the VE count of the $Sc_2Ir_{6-x}Pd_xB$ (blue) and $Sc_2Ir_{6-x}Ni_xB$ (green) series (x = 0−6; VE = 63−69). The lattice parameters of the ternary compounds ($ScPd_3B_x$ and $ScNi_3B_x$), which do not crystallize in the superstructure, have been doubled (asterisk) for comparison. The error bars of the lattice parameters are all ±0.002 or less and thus lie within the data points.

as a function of the number of VE per formula unit. For the x = 6 composition, for which the simple cubic structure was found, a was doubled. As can be seen, a linear increase of the lattice parameters with increasing VE (or increasing Pd content) is observed, and Vegard behavior is found for the compositions (x = 0−4) for which superstructure reflections were unambiguously observed. The lattice parameter of the Pd-richest quaternary composition (x = 5) deviates from Vegard behavior, and it is unexpectedly smaller than that of the x = 4 composition. A further increase of Pd en route to the x = 6 ternary phase also leads to an unexpected decrease of a (see also Table S1 in the Supporting Information, SI). This behavior is contrary to the atomic size change when the larger Pd is substituted for the smaller Ir. A similar observation was made by Zeiringer et al. in the series $CeRh_{3-x}Pd_xB_{0.5}$[19] upon increasing x from 2.5 to 3. It was associated with a change in the Ce valence state from a mixed-valence state to Ce^{3+}. However, the explanation cannot be applied for $Sc_2Ir_{6-x}Pd_xB$ because Sc does not exist either in a mixed-valence state or as Sc^{4+}. In the $Sc_2Ir_{6-x}Ni_xB$ series, a deviation from Vegard's law is also found at higher unit cell volumes. An explanation of this behavior is not available at the moment, and subsequent experimental investigations (for example, electron diffraction) of the whole series are planned for the future.

The crystal structures of the Sc_2Ir_6B phase and the quaternary solid solution $Sc_2Ir_{6-x}Pd_xB$ (x = 1−5) were investigated by Rietveld refinement and single-crystal analysis, respectively. For the Sc_2Ir_6B composition, a high-quality powder pattern was measured and Rietveld refinement was carried out using the single-crystal model of the known Zr_2Ir_6B[11] phase (see Table 1). The refinement confirmed the positions of all atoms at their respective Wyckoff sites (Sc at 8c, Ir at 24e, and B at 4a). The fitted pattern (see Figure 4) clearly indicates that the superstructure reflections have been well modeled (see the enlarged part of the figure), thus confirming the ordering of boron in this phase. As a consequence, the formerly known

Table 1. Rietveld Refinement Details of Sc_2Ir_6B and $Sc_2Ir_{3.9(1)}Ni_{2.1(1)}B$

refined composition	Sc_2Ir_6B	$Sc_2Ir_{3.9(1)}Ni_{2.1(1)}B$
loaded composition	Sc_2Ir_6B	$Sc_2Ir_4Ni_2B$
space group, Z	$Fm\bar{3}m$, 4	$Fm\bar{3}m$, 4
a (Å)	7.9653(5)	7.8940(5)
V (Å^3)	505.37(5)	491.91(5)
calcd density (g/cm^3)	16.481	13.150
2θ range (deg)	5−85	5−85
refinement method	least-squares method	
profile function	pseudo-Voigt	
structural model	Zr_2Ir_6B[11]	$Sc_2Ir_{2.1(3)}Pd_{3.9(3)}B$ single-crystal data (Table 1)
x, y, z (site 24e)	0.2577(3), 0, 0	0.2581(3), 0, 0
SOF (site 24e)	1 (Ir)	0.65(2)/0.35 (Ir/Pd)
R_p	0.0310	0.0288
R_{Bragg}	0.0172	0.0098
CSD number[a]	428533	428532

[a]More details on the structure determination may be obtained from the Fachinformationszentrum Karlsruhe (e-mail: crysdata@fiz-karlsruhe.de), Eggenstein-Leopoldshafen, Germany, upon quoting the given CSD depository.

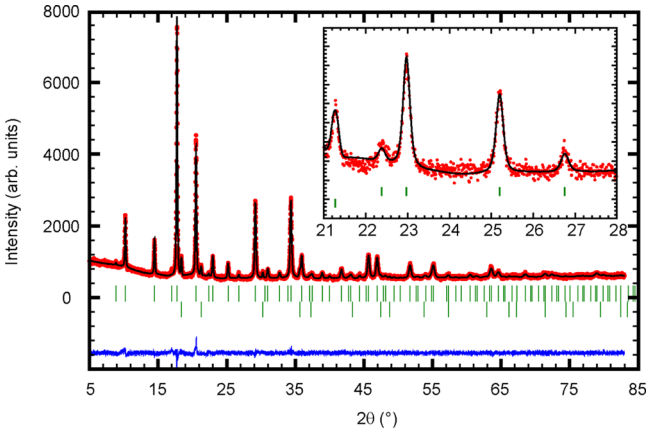

Figure 4. Rietveld refinement of the powder pattern (Mo Kα radiation) of Sc_2Ir_6B showing measured (red) and fitted (black) intensities, the position of the Bragg reflections (green) for Sc_2Ir_6B (top) and for the minor Ir phase, and the difference intensity curve (blue). The inset shows a magnification of a part of the pattern, in which two superstructure reflections are positioned.

nonstoichiometric $ScIr_3B_{1-y}$[4] should be reformulated, for y = 0.5, as stoichiometric Sc_2Ir_6B. This finding also confirms the above prediction that this 63 VE phase should also crystallize with the double-perovskite-like Ti_2Rh_6B-type structure.

Next, we will examine the crystal structure of the quaternary solid solution, $Sc_2Ir_{6-x}Pd_xB$ (x = 1−4). The composition $Sc_2Ir_2Pd_4B$, for which single crystals were found, should allow the detailed determination of the crystal structure of this solid solution. The structure solution indicated two metal sites, 8c and 24e, which were successfully filled with Sc and a mixture of Pd and Ir, respectively. After a few refinement cycles, the 4a site appeared in the difference Fourier map and was assigned to B, which led to a significantly better refinement with final R values of R1 = 0.0318 and wR2 = 0.0574 for all 89 independent reflections. The metal mixture on the 24e site accounts for an Ir/

DOI: 10.1021/acs.inorgchem.5b00292
Inorg. Chem. 2015, 54, 4056−4063

Pd ratio of 0.34(4)/0.66(4), which leads to a formula sum of $Sc_2Ir_{2.1(3)}Pd_{3.9(3)}B$ in very good agreement with the loaded composition. Details of the single-crystal refinement are listed in Table 2. Table 3 contains the atomic and thermal displacement parameters. Table 4 lists selected interatomic distances. This single-crystal result shows that Pd has indeed substituted Ir in the ternary boride Sc_2Ir_6B at the Ir site (24e) only and that the predicted VE count (67 VE) for this composition is confirmed. For the predicted 68 VE composition, the above-mentioned powder X-ray analysis and Rietveld refinement (not shown) confirm that the double-perovskite-like structure was achieved. This finding confirms the predicted upper VE limit of 68 VE, in particular because for the 69 VE ternary phase no superstructure reflections were found, in accordance with the already reported result.[1a] According to these results, the experimentally found VE range for the $Sc_2Ir_{6-x}Pd_xB$ (x = 0−6) series varies from 63 to 68 VE and thus lies within the pseudogap range (61−68 VE), as predicted.

Table 2. Crystallographic and Single-Crystal Structure Data of $Sc_2Ir_{2.1(3)}Pd_{3.9(3)}B$

formula	$Sc_2Ir_{2.1(3)}Pd_{3.9(3)}B$
space group, Z	$Fm\bar{3}m$, 4
fw (g/mol)	915.66
cryst size (mm^3)	0.06 × 0.02 × 0.01
F(000)	1547
lattice parameters	
a (Å)	8.070(3)
V (Å^3)	525.6(3)
calcd density (g/cm^3)	11.572
abs coeff (mm^{-1})	67.293
T_{min}, T_{max}	0.1071, 0.5526
θ range (deg)	5.05−35.75
hkl range	$-10 \le h \le 13$
	$-13 \le k \le 11$
	$-13 \le l \le 12$
no. of reflns, R_{int}	1408, 0.0404
no. of indep reflns	89
no. of param	7
R1, wR2 (all I)	0.0318, 0.0574
R1, wR2 ($I > 2\sigma$)	0.0252, 0.0514
GOF	1.183
diff peak/hole (e/Å^3)	−1.574/2.466
CSD number[a]	428531

[a]More details on the structure determination may be obtained from the Fachinformationszentrum Karlsruhe (e-mail: crysdata@fiz-karlsruhe.de), Eggenstein-Leopoldshafen, Germany, upon quoting the given CSD depository.

Table 4. Interatomic Distances (Å) of Sc_2Ir_6B, $Sc_2Ir_{3.9(2)}Ni_{2.1(2)}B$, and $Sc_2Ir_{2.1(3)}Pd_{3.9(3)}B$ (T = Ir, Ir/Ni, or Ir/Pd)

atom 1	atom 2	count	Sc_2Ir_6B	$Sc_2Ir_{3.9(2)}Ni_{2.1(2)}B$	$Sc_2Ir_{2.1(3)}Pd_{3.9(3)}B$
Sc1	T2	12	2.8168(1)	2.7917(1)	2.8538(7)
T2	B3	1	2.053(1)	2.037(1)	2.076(1)
	T2 (T_6)	4	2.729(1)	2.701(1)	2.7699(9)
	Sc1	4	2.8168(1)	2.7917(1)	2.8538(7)
	T2 (T_6B)	4	2.903(1)	2.881(1)	2.937(1)
B3	T2	6	2.053(1)	2.037(1)	2.0764(8)

$Sc_2Ir_{6-x}Ni_xB$ Series. In the previous section, it is shown that a partial substitution of Ir by Pd in Sc_2Ir_6B leads to new double-perovskite-like compositions in the 63−68 VE range, as predicted by the pseudogap analysis above. The same VE range can be obtained if Ni is substituted for Ir instead of the isoelectronic Pd. While Pd has a larger atomic radius than Ir, Ni is much smaller, indicating opposite size-dependent substitution behaviors.

The powder X-ray diffractograms of all members of the $Sc_2Ir_{6-x}Ni_xB$ series (x = 1−6) have been analyzed. The Ir-containing ternary phase Sc_2Ir_6B, the X-ray diffratogram of which shows superstructure reflections, has been discussed in the previous section. For the other ternary phase of the series, i.e., with x = 6, no superstructure reflections could be observed, in accordance with the literature,[16] and it also confirms the theoretical prediction of unstable double-perovskite-like phases with 69 VE. Also, its powder diffractogram contains broad peaks, indicating a phase width. Analysis of the powder diffractograms for x = 1−5 shows that in all cases a double-perovskite-like structure was obtained (see Figure 5). In some of these compositions (x = 1, 4, and 5), additional reflections are present, which could be assigned to the minor phase $ScIr_{2-x}Ni_x$ ($MgCu_2$-type structure, space group $Fd\bar{3}m$).[18] The inset of Figure 5 shows a magnified area in which two of the superstructure reflections are highlighted. Two observations prove that Ni has really been stepwise introduced in the structure. First, the notable shift of the reflections in the direction of larger 2θ values shows that the lattice parameters decrease with increasing Ni content. The trend of the lattice parameter over the whole series is also plotted in Figure 3. Similar to the $Sc_2Ir_{6-x}Pd_xB$ series, Vegard behavior is found for four out of the six compositions, and only the two having the largest volumes deviate from this behavior (see also Table S1 in the SI). As mentioned above already, no explanation is available for this deviation at the moment. The second observation concerns the intensities of the superlattice reflections. The intensities of these reflections increase with increasing Ni content. This becomes apparent if we compare a main reflection with a superstructure reflection, as highlighted in Figure 5. The reflection indexed as 422, which is also present in the simple perovskite (there indexed as 211), is highlighted in green, while the adjacent superstructure reflection (indexed as 333) is highlighted in red. It can be clearly seen that the intensity of the superstructure reflection is increasing with increasing x, while that of 422 (main reflection) remains constant. Simulated diffraction patterns, in which these two reflections are high-

Table 3. Atomic Coordinates, Site Occupation Factors (SOFs), and Displacement Parameters of $Sc_2Ir_{2.1(3)}Pd_{3.9(3)}B$ (U_{12}, U_{13}, and U_{23} = 0)

name	site	x	y	z	SOF	U_{eq}	U_{11}	U_{22}	U_{33}
Sc1	8c	0.25	0.25	0.25	1	0.011(2)	0.011(2)	0.011(2)	0.011(2)
Ir2	24e	0.25730(7)	0	0	0.34(4)	0.0075(2)	0.0068(3)	0.0078(2)	0.0078(2)
Pd2	24e	0.25730(7)	0	0	0.66(4)	0.0075(2)	0.0068(3)	0.0078(2)	0.0078(2)
B3	4a	0	0	0	1	0.014(6)	0.014(6)	0.014(6)	0.014(6)

DOI: 10.1021/acs.inorgchem.5b00292
Inorg. Chem. 2015, 54, 4056−4063

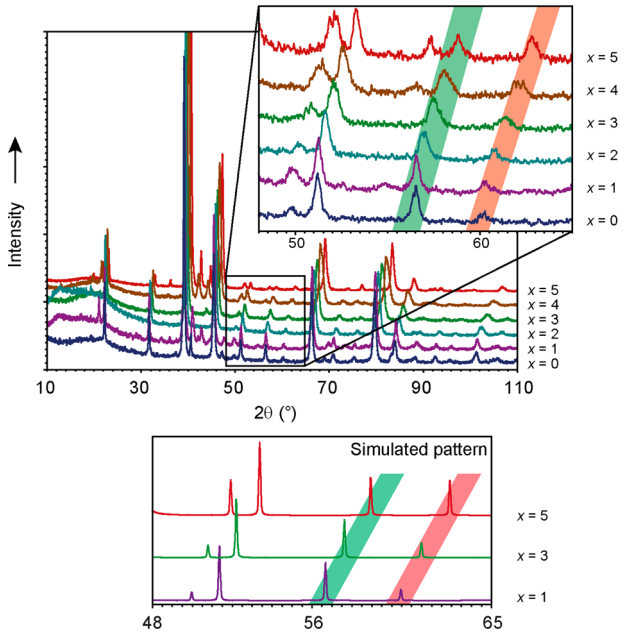

Figure 5. (top) Powder patterns (Cu Kα_1 radiation) of the $Sc_2Ir_{6-x}Ni_xB$ series (x = 1−5). A 2θ range is magnified, in which one main reflection (422) and one superstructure reflection (333) are highlighted. (bottom) Simulated diffraction patterns (for x = 1, 3 and 5), which also highlight these two reflections.

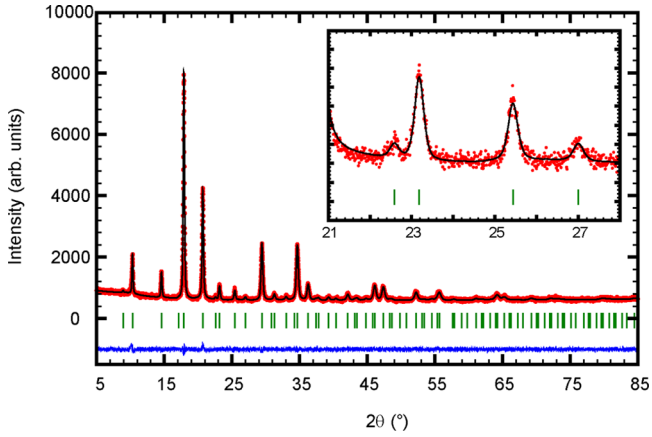

Figure 6. Rietveld refinement of the powder pattern (Mo Kα radiation) of $Sc_2Ir_4Ni_2B$ showing measured (black) and fitted (red) intensities, the position of the Bragg reflections (green), and the difference intensity curve (blue). The inset shows a magnification of a part of the pattern, in which two superstructure reflections are positioned.

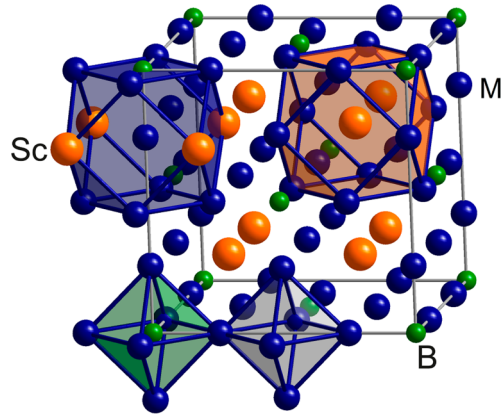

Figure 7. Perspective view of the unit cell of the structure of the new $Sc_2Ir_{6-x}M_xB$ (x = 0−5; M = Pd, Ni) series. The coordination polyhedra of the different atoms as well as the filled and empty Ir_6 or $(Ir/M)_6$ octahedra are highlighted.

lighted, show the same characteristics (Figure 5, lower diagram). This indicates that the superstructure reflections should be clearly seen in compositions with high Ni content including the 69 VE ternary "Sc_2Ni_6B" phase. However, as indicated above already, no superstructure could be found in its powder diffractogram. This confirms not only the nonstoichiometric nature of this phase but also the theoretical prediction of unstable double-perovskite-like phases with VE > 68. Furthermore, the nonstoichiometric nature of the isoelectronic Pd-based ternary phase, which has a far higher unit cell volume than the Ni-based one (see Figure 3), indicates that the occurrence of a superstructure reflection, i.e., boron ordering, is mostly governed by electronic factors rather than by size effects. To verify this hypothesis, we plan in the near future to synthesize the isoelectronic solid solution $Sc_2Pd_{6-x}Ni_xB$ (x = 1−5), for which no superstructure reflection is expected because all members have 69 VE.

The crystal structure and composition of the quaternary $Sc_2Ir_{6-x}Ni_xB$ (x = 1−5) series were refined by the Rietveld method using as an example a high-quality powder pattern for the $Sc_2Ir_4Ni_2B$ composition (see Figure 6 and Table 1). The $Sc_2Ir_{2.1(3)}Pd_{3.9(3)}B$ single-crystal structure was used as the starting model but with Pd replacing Ni. The mixed-occupancy refinement on the 24e site leads to an Ir/Ni ratio of 0.65(2)/0.35(2) and therefore to the nearly ideal $Sc_2Ir_{3.9(1)}Ni_{2.1(1)}B$ formula sum, as expected from this single-phase sample.

Crystal Chemistry. Figure 7 shows a perspective view of the unit cell of the new $Sc_2Ir_{6-x}M_xB$ (x = 0−5; M = Pd, Ni) series. They crystallize as substitutional variants of the double-perovskite-like Ti_2Rh_6B-type structure.[8] The structure of the ternary Sc_2Ir_6B is isotypic to Ti_2Rh_6B and Zr_2Ir_6B, which have been described in detail before.[8,11] The structure of the new quaternary $Sc_2Ir_{6-x}M_xB$ (x = 1−5; M = Pd, Ni) series may simply be derived from that of the ternary Sc_2Ir_6B by replacing Ir in the structure by the Ir/M (M = Pd, Ni) mixture (see Figure 7). As a consequence, empty $(Ir/M)_6$ and B-filled $(Ir/M)_6B$ octahedra, which are corner-connected to a 3D network, result. The Ir/M mixture is coordinated by a cuboactahedron of four Sc and eight Ir/M atoms and one B atom centering one quadratic face (Figure 7). Sc also has a coordination sphere in the form of a cuboactahedron of Ir/M atoms only.

The distances in these compounds follow the trend of the lattice parameters. All distances increase with increasing lattice parameters, as exemplified for Sc_2Ir_6B, $Sc_2Ir_{3.9(1)}Ni_{2.1(1)}B$, and $Sc_2Ir_{2.1(3)}Pd_{3.9(3)}B$ (see Table 4). The distances of Sc_2Ir_6B are comparable to those reported for Zr_2Ir_6B,[11] as expected, because Zr and Sc nearly have the same atomic radius. For $Sc_2Ir_{3.9(1)}Ni_{2.1(1)}B$ and $Sc_2Ir_{2.1(3)}Pd_{3.9(3)}B$, the effect of different atomic radii is obvious; those of the Ni-based phase are significantly smaller as opposed to larger ones for the Pd-based phase (see Table 4). The distances in the $(Ir/M)_6$ octahedron differ, depending on whether the octrahedron is filled with B or not. The edge length, and hence the volume of the B-filled octahedron, is larger. For example, in $Sc_2Ir_{2.1(3)}Pd_{3.9(3)}B$, the distance is 2.7699(9) Å in the empty octahedron and 2.937(1) Å in the B-filled one. The different length comes from the displacement of the Ir/Pd atoms on site 24e away from the

DOI: 10.1021/acs.inorgchem.5b00292
Inorg. Chem. 2015, 54, 4056−4063

centered position (0, 0, $^1/_4$). In fact, if this particular position is occupied, the small perovskite structure will occur. Actually, the presence and intensity of the superstructure reflections in the diffraction pattern arise mainly from this displacement. Although the displacement is caused by the ordering of boron, their actual contribution to the intensity of the superstructure reflections is only small because of the weak scattering factor of boron, which is the main reason why it is difficult to find these superstructure reflections by diffraction methods. Theoretical analysis of the pseudogap as a guide for the synthesis of new compositions, as done in this work, will therefore be of tremendous importance for the discovery of new double-perovskite-like borides in the future.

CONCLUSION

In this contribution, we have reported on the synthesis and characterization of the two perovskite-like borides series $Sc_2Ir_{6-x}Pd_xB$ and $Sc_2Ir_{6-x}Ni_xB$ (x = 0−6). They have been synthesized by arc melting the elements. Theoretical analyses of the DOSs and COHPs of the ternary phases Sc_2M_6B (M = Ir, Pd, Ni) have revealed the presence of pseudogaps near their Fermi levels between 61 and 68 VE. This led to the prediction of new phases in the double-perovskite-like Ti_2Rh_6B-type structure (space group $Fm\bar{3}m$, Z = 4). Boron ordering was confirmed by the observation of superstructure reflections in the powder diffractograms of $Sc_2Ir_{6-x}Pd_xB$ and $Sc_2Ir_{6-x}Ni_xB$ (x = 0−5; VE 63−68). Single-crystal and Rietveld refinement results confirm and extend these findings because, in the quaternary compositions, Ir and Pd (or Ni) were found to mix on the 24e Wyckoff site only.

EXPERIMENTAL PART

Synthesis and Energy-Dispersive X-ray (EDX) Analysis. Polycrystalline samples and single crystals of the $Sc_2Ir_{6-x}Pd_xB$ and $Sc_2Ir_{6-x}Ni_xB$ series were synthesized by arc melting the elements in a water-cooled copper crucible under an argon atmosphere using a tungsten tip as a second electrode. The starting materials, scandium, (powder, >99.9%, Chempur), iridium (powder, 99.95%, Alfa Aesar), palladium (Haraeus, 99.9%), nickel (Fluka, 99.99%), and boron (amorphous powder, 95−97%, ABCR, or crystalline pieces, 99.999%, Alfa Aesar), were weighed in the respective atomic ratios, pressed into pellets, and arc-melted under argon until homogeneous melting; the argon was purified prior to use over silica gel, molecular sieves, and titanium sponge (950 K). The reaction products were remelted to ensure good homogeneity of the samples. Weight losses during the melting process were negligible. A silver-like product with metallic luster was obtained with several single crystals suitable for X-ray structure analysis. The samples were stable in air as a compact bulk as well as a finely ground powder.

The purity of each sample was checked by powder X-ray diffraction using Cu Kα_1 radiation (λ = 1.54059 Å). The lattice parameters were refined on the basis of powder data with the program *WinXPOW*.[20] The presence of all metals were checked by EDX analysis on a high-resolution low-energy scanning electron microscope of the type LEO 1530 (Oberkochen, Germany) equipped with an EDX system of the type INCA (Oxford, England).

Rietveld Refinement. A high-quality powder diffractogram was measured (2θ variation of 0.01°/step) on a STOE STADI MP diffractometer equipped with a position-sensitive detector using monochromatized Mo Kα_1 radiation (λ = 0.71073 Å). The crystal structure was refined by full-matrix least-squares refinement implemented in the *FULLPROF* program.[21]

Single-Crystal Refinement. Single crystals of suitable size were fixed on top of glass capillaries, and X-ray data were collected on a CCD single-crystal diffractometer (Bruker SMART APEX) with graphite-monochromatized Mo Kα radiation (λ = 0.71073 Å). The X-ray intensities were corrected with respect to absorption using a semiempirical procedure.[22] The crystal structure was solved by direct methods and refined by full-matrix least-squares refinement (based on F^2) using the *SHELX* program package.[23]

Density Functional Theory (DFT) Calculations. The DOSs of the hypothetical phases Sc_2Ir_6B (63 VE), Sc_2Pd_6B (69 VE), and Sc_2Ni_6B (69 VE) have been calculated by means of DFT.

In a first step, the lowest-energy structures were determine by the Vienna ab initio simulation package (VASP) using plane-wave basis sets and projector-augmented-wave potentials.[24] Correlation and exchange were treated with the generalized gradient approximation in the parametrization of Perdew, Burke, and Ernzernhof.[25]

On the electronically and structurally relaxed structures, first-principles scalar-relativistic electronic structure calculations were performed by means of the TB-LMTO representation and the atomic sphere approximation, as implemented in the *STUTTGART TB-LMTO-ASA 4.7* program.[26] The electronic energy was calculated using the von Barth and Hedin parametrization of the local exchange-correlation potential.[27] For details concerning the calculation steps, see, for example, ref 15. Chemical bonding analyses were based on the DOSs and COHPs.[28]

ASSOCIATED CONTENT

Supporting Information

Table S1 containing the lattice parameters of the $Sc_2Ir_{6-x}M_xB$ (M = Pd, Ni) series, Figure S1 showing the klassengleiche group−subgroup relationship (Bärnighausen tree) between the simple ($ScIr_3B_x$) and double (Sc_2Ir_6B) cubic perovskite-like structures, and a PDF of the X-ray crystallographic data. This material is available free of charge via the Internet at http://pubs.acs.org.

AUTHOR INFORMATION

Corresponding Author

*E-mail: Boniface.Fokwa@ac.rwth-aachen.

Author Contributions

†M.H. and J.P.S. contributed equally to this work.

Notes

The authors declare no competing financial interest.

ACKNOWLEDGMENTS

We thank the Deutsche Forschungsgemeinschaft for financial support as well as for awarding the Heisenberg fellowship to B.P.T.F. and the IT Center of RWTH Aachen University for providing calculation power and time.

REFERENCES

(1) (a) Schaak, R. E.; Avdeev, M.; Lee, W.-L.; Lawes, G.; Zandbergen, H. W.; Jorgensen, J. D.; Ong, N. P.; Ramirez, A. P.; Cava, R. J. *J. Solid State Chem.* **2004**, *177*, 1244−1251. (b) Takahashia, T.; Iskandar, R.; Munnik, F.; Music, D.; Mayer, J.; Schneider, J. M. *J. Alloys Compd.* **2012**, *540*, 75−80. (c) Hossain, M. A.; Ali, M. S.; Parvin, F.; Islam, A. *Comput. Mater. Sci.* **2013**, *73*, 1−8. (d) Shao, D.; Lu, W.; Tong, P.; Lin, S.; Lin, J.; Sun, Y. *J. Phys. Soc. Jpn.* **2014**, *83*, 054704−054714.

(2) (a) Takei, H.; Kobayashi, N.; Yamauchi, H.; Shishido, T.; Fukase, T. *J. Less-Common Met.* **1986**, *125*, 233−237. (b) Sahara, R.; Shishido, T.; Nomura, A.; Kudou, K.; Okada, S.; Kumar, V.; Nakajima, K.; Kawazoe, Y. *Phys. Rev. B* **2006**, *73*, 1841021−1841029. (c) Music, D.; Schneider, J. M. *Appl. Phys. Lett.* **2006**, *89*, 121914−121917.

(3) Shishido, T.; Ye, J.; Kudou, K.; Okada, S.; Obara, K.; Sugawara, T.; Oku, M.; Wagatsuma, K.; Horiuchi, H.; Fukuda, T. *J. Alloys Compd.* **1999**, *291*, 52−56.

(4) Holleck, H. *J. Less-Common Met.* **1977**, *52*, 167−172.

(5) Rogl, P.; Nowotny, H. *J. Less-Common Met.* **1979**, *67*, 41−50.

(6) Rogl, P.; Delong, L. *J. Less-Common Met.* **1983**, *91*, 97−106.

(7) Shishido, T.; Ye, J.; Kudou, K.; Okada, S.; Obara, K.; Sugawara, T.; Oku, M.; Wagatsuma, K.; Horiuchi, H.; Fukuda, T. *J. Alloys Compd.* **1999**, *291*, 52−56.

DOI: 10.1021/acs.inorgchem.5b00292
Inorg. Chem. 2015, 54, 4056−4063

(8) Fokwa, B. P. T.; Eck, B.; Dronskowski, R. *Z. Kristallogr.* **2006**, *221*, 445−449.
(9) (a) Yubuta, K.; Nomura, A.; Nakajima, K.; Shishido, T. *J. Alloys Compd.* **2006**, *426*, 308−311. (b) Yubuta, K.; Nomura, A.; Yamamura, T.; Shishido, T. *J. Alloys Compd.* **2008**, *451*, 301−304.
(10) Yubuta, K.; Nomura, A.; Nakajima, K.; Shishido, T. *J. Alloys Compd.* **2009**, *471*, 341−346.
(11) Hermus, M.; Fokwa, B. P. T. *J. Solid State Chem.* **2010**, *183*, 784−788.
(12) Hermus, M.; Geier, D.; Fokwa, B. P. T. *Z. Anorg. Allg. Chem.* **2012**, *638*, 49−52.
(13) Hermus, M.; Fokwa, B. P. T. *Eur. J. Inorg. Chem.* **2012**, 4877−4884.
(14) Fokwa, B. P. T.; Hermus, M. *Inorg. Chem.* **2011**, *50*, 3332−3341.
(15) Hermus, M.; Fokwa, B. P. T. *Eur. J. Inorg. Chem.* **2014**, 3085−3094.
(16) (a) Shishido, T.; Kudou, K.; Sasaki, T.; Okada, S.; Ye, J.; Iizumi, K.; Nomura, A.; Sugawara, T.; Obara, K.; Tanaka, M.; et al. *Jpn. J. Appl. Phys.* **2003**, *42*, 7464−7466. (b) Shishido, T.; Kudou, K.; Sasaki, T.; Okada, S.; Ye, J.; Iizumi, K.; Nomura, A.; Sugawara, T.; Obara, K.; Tanaka, M.; et al. *J. Alloys Compd.* **2004**, *383*, 294−297.
(17) Yeremenko, V. N.; Khorujaya, V. G.; Martsenyuk, P. S. *J. Alloys Compd.* **1994**, *204*, 83−87.
(18) FindIt, Inorganic Crystal Structure Database, version 1.9.3, 2013.
(19) Zeiringer, I.; Sereni, J. G.; Berisso, M. G.; Yubuta, K.; Rogl, P.; Grytsiv, A.; Bauer, E. *Mater. Res. Express* **2014**, *1*, 016101−016118.
(20) *WinXPOW*, version 2.23; STOE & Cie GmbH: Darmstadt, Germany, 2008.
(21) Rodriguez-Carvajal, J. *Physica B: Condensed Matter* **1993**, *192*, 55−69.
(22) Sheldrick, G. M. *SADABS*; University of Göttingen: Göttingen, Germany, 2001.
(23) Sheldrick, G. M. *Acta Crystallogr.* **2008**, *A64*, 112−122.
(24) Kresse, G.; Joubert, D. *Phys. Rev. B* **1999**, *59*, 1758−1775.
(25) Perdew, J. P.; Burke, K.; Ernzerhof, M. *Phys. Rev. Lett.* **1996**, *77*, 3865−3868.
(26) (a) Jepsen, O.; Andersen, O. K. *The STUTTGART TB-LMTO program*; Max-Planck-Institut für Festkörperforschung: Stuttgart, Germany, 2000. (b) Andersen, O. K. *Phys. Rev. B* **1975**, *12*, 3060. (c) Andersen, O. K.; Jepsen, O. *Phys. Rev. Lett.* **1984**, *53*, 2571−2574. (d) Andersen, O. K.; Skriver, H.; Nohl, H.; Johansson, B. *Pure Appl. Chem.* **1980**, *52*, 93−118.
(27) Perdew, J. P.; Wang, Y. *Phys. Rev. B* **1992**, *45*, 13244−13249.
(28) Dronskowski, R.; Blöchl, P. E. *J. Phys. Chem.* **1993**, *97*, 8617−8624.

DOI: 10.1021/acs.inorgchem.5b00292
Inorg. Chem. 2015, 54, 4056−4063